

Specular Manifold Sampling for Rendering High-Frequency Caustics and Glints

TIZIAN ZELTNER, École Polytechnique Fédérale de Lausanne (EPFL), Switzerland

ILIYAN GEORGIEV, Autodesk, United Kingdom

WENZEL JAKOB, École Polytechnique Fédérale de Lausanne (EPFL), Switzerland



Fig. 1. Rendering of a shop window featuring a combination of challenging-to-sample light transport paths with specular-diffuse-specular (“SDS”) inter-reflection: the two golden normal-mapped pedestals are illuminated by spot lights and project intricate caustic patterns following a single reflection from the metallic surface, while the transparent center pedestal generates caustics via double refraction. The glinty appearance of the shoes arises due to specular microgeometry encoded in a high-frequency normal map. This image was rendered by an ordinary unidirectional path tracer using our new specular manifold sampling strategy. The remaining noise is due to indirect lighting by caustics, which is not explicitly sampled by our technique. The background image is “Hexactinellae” from *Art Forms in Nature* by Ernst Haeckel.

Scattering from specular surfaces produces complex optical effects that are frequently encountered in realistic scenes: intricate caustics due to focused reflection, multiple refraction, and high-frequency glints from specular microstructure. Yet, despite their importance and considerable research to this end, sampling of light paths that cause these effects remains a formidable challenge.

In this article, we propose a surprisingly simple and general sampling strategy for specular light paths including the above examples, unifying the previously disjoint areas of caustic and glint rendering into a single framework. Given two path vertices, our algorithm stochastically finds a specular subpath connecting the endpoints. In contrast to prior work, our

method supports high-frequency normal- or displacement-mapped geometry, samples specular-diffuse-specular (“SDS”) paths, and is compatible with standard Monte Carlo methods including unidirectional path tracing. Both unbiased and biased variants of our approach can be constructed, the latter often significantly reducing variance, which may be appealing in applied settings (e.g. visual effects). We demonstrate our method on a range of challenging scenes and evaluate it against state-of-the-art methods for rendering caustics and glints.

CCS Concepts: • Computing methodologies → Rendering.

Additional Key Words and Phrases: Specular light paths, SDS paths, Caustics, Glints

ACM Reference Format:

Tizian Zeltner, Iliyan Georgiev, and Wenzel Jakob. 2020. Specular Manifold Sampling for Rendering High-Frequency Caustics and Glints. *ACM Trans. Graph.* 39, 4, Article 149 (July 2020), 15 pages. <https://doi.org/10.1145/3386569.3392408>

Authors’ addresses: Tizian Zeltner, École Polytechnique Fédérale de Lausanne (EPFL), Switzerland, tizian.zeltner@epfl.ch; Iliyan Georgiev, Autodesk, United Kingdom, iliyan.georgiev@autodesk.com; Wenzel Jakob, École Polytechnique Fédérale de Lausanne (EPFL), Switzerland, wenzel.jakob@epfl.ch.

© 2020 Copyright held by the owner/author(s). Publication rights licensed to ACM. This is the author’s version of the work. It is posted here for your personal use. Not for redistribution. The definitive Version of Record was published in *ACM Transactions on Graphics*, <https://doi.org/10.1145/3386569.3392408>.

1 INTRODUCTION

Efficient simulation of the physical process of light transport and scattering constitutes one of the classic problems in the field of computer graphics. Over the past decades, research on this challenging problem has gravitated towards methods that perform Monte Carlo integration over high-dimensional sets of light transport paths, fueling the development of a toolbox of sophisticated path sampling strategies that are now in widespread use. While Monte Carlo rendering has been extremely successful in both industry and academia, there are many settings where these methods are surprisingly brittle and subject to catastrophically poor convergence.

One particularly problematic case are scenes containing *specular paths*, i.e., paths involving chains of interactions with smooth metallic or refractive surfaces. Their constrained nature makes such light paths difficult to find: at specular interfaces, light must satisfy the law of reflection or Snell’s law, which drastically lowers the probability of sampling a valid configuration connecting the camera to a light source. Caustics or glittery surfaces that exhibit random patterns of highlights due to specular micro-geometry are visually striking examples of such specular paths, though they are often much more subtle while still having a negative effect on overall convergence. The large family of *specular-diffuse-specular* (“SDS”) paths with only a single diffuse vertex surrounded by specular chains simply cannot be found at all and is normally absent in rendered images. The caustics seen through the shop window in Fig. 1 are an example of this configuration—they are only visible thanks to the proposed sampling strategy. The glints on the shoes are even more challenging and involve *only specular vertices*: a point spotlight, perfectly specular microstructure, the glass window, and a pinhole camera.

Faced with these challenges, research in the last two decades has produced a large set of tailored methods that are each able to render specific types of specular paths. However, no existing method tackles the general case, and every approach brings along an intrinsic set of limitations: for instance, bidirectional sampling [Lafortune and Willems 1993; Veach and Guibas 1995a] from cameras and light sources often improves convergence, but does not help with glints or SDS paths, and tends to be brittle when the two partial paths only rarely find each other¹. Biased methods [Jensen 1996; Hachisuka and Jensen 2009] that relax the problem via spatial smoothing support SDS paths and greatly improve convergence but do not handle glints and introduce blur that is often undesirable. Specialized glint rendering methods for normal-mapped surfaces [Yan et al. 2014, 2016] are excellent at their task but do not help with other types of specular paths and require many gigabytes of memory to hold precomputed data structures. Finally, path sampling techniques based on specular manifolds [Jakob and Marschner 2012; Hanika et al. 2015a] are very powerful in theory but tend to be extremely fragile in practice, particularly when the scene geometry features high-frequency detail.

In this paper, we present a remarkably simple technique for sampling specular chains connecting two specified shading points—including glints and SDS paths—in an unbiased manner. Our approach builds on the theory of specular manifolds but significantly improves its practicality in formerly challenging cases, e.g. when

¹e.g., in the common setting when the camera is inside a building that is lit from outside.

working with high-frequency displaced or normal-mapped geometry. Concretely, our contributions are:

- (1) A unified manifold sampling strategy for rendering reflective and refractive caustics.
- (2) A specialized variant for rendering glints, which reduces memory usage hundred-fold compared to prior work.
- (3) A biased variant of the method with reduced variance.
- (4) A two-pass sampling strategy for normal-mapped surfaces.
- (5) Changes to the specular manifold constraints of Jakob and Marschner [2012] that improve robustness and convergence.

The main limitation of our sampling technique is that variance increases significantly for longer specular chains, hence our experiments mainly focus on short chains with 1 or 2 vertices. That said, our approach is highly extensible, and we believe that future work could address this limitation.

We show how our method can be deployed in a unidirectional path tracer and compare its performance to prior work. We will release our implementation as open source to ensure reproducibility.

2 PRIOR WORK

Path tracing, proposed in Kajiya’s seminal 1986 paper, is the foundation of an extensive body of work on unbiased Monte Carlo rendering including later bidirectional extensions [Lafortune and Willems 1993; Veach and Guibas 1995a] and specialized guiding strategies that exploit past observations to improve the quality of generated samples [Vorba et al. 2014; Müller et al. 2017; Simon et al. 2018]. However, even state-of-the-art methods with both bidirectional sample generation and guiding fail to find SDS paths and produce high variance when the scene contains objects with glinty microstructure.

Methods based on photon maps [Jensen 1996] are able to resolve the issues with SDS paths by introducing spatial blur that relaxes the original problem. These methods emit photons from light sources in a first pass that are stored on surfaces and queried in a secondary density estimation phase. Later work has shown how very large number of photons can be sampled progressively [Hachisuka and Jensen 2009], and how photon lookups can be incorporated in bidirectional rendering algorithms [Georgiev et al. 2012; Hachisuka et al. 2012] combining many different strategies using multiple importance sampling [Veach and Guibas 1995b]. While photon maps are an excellent choice for certain path classes, they can introduce objectionable blur, and they do not handle important cases including caustics on non-diffuse surfaces or glints. The path space can also be selectively mollified to introduce bias only for path types that were otherwise impossible to sample [Kaplanyan and Dachsbaecher 2013]. In contrast, our work focuses on general path sampling in the original non-relaxed problem.

Fermat’s principle states that specular paths are *extremal*, i.e., they locally maximize or minimize the time that light requires to travel from one end to the other. One way of generating such paths thus entails optimizing path length or solving an equivalent root finding problem. This idea was pioneered by Mitchell and Hanrahan [1992], who render caustics from implicitly defined curved reflectors using interval arithmetic and Newton-Raphson iteration to find 1-bounce specular reflections connecting a given pair of vertices. We also experimented with a similar approach in an early stage of this

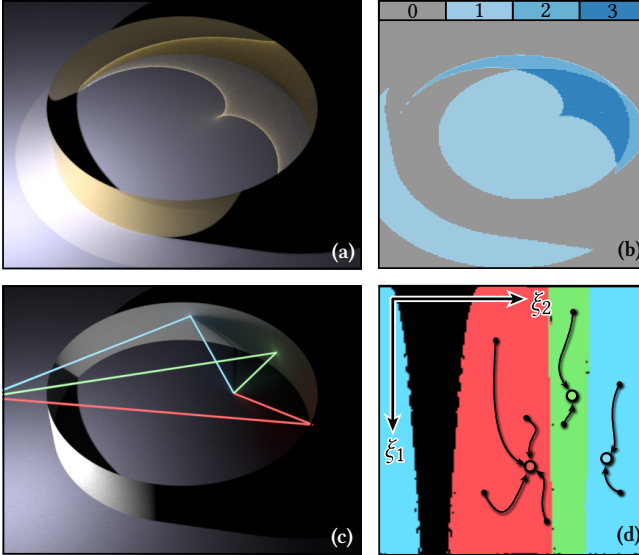


Fig. 4. (a): Multiple solutions of the specular path constraint form a superposition of caustics in the RING scene. (b): Color map showing the number of solutions at each shading point. (c): The three solution paths at a particular point. (d): The basins of convergence (in primary sample space) corresponding to those solution paths. All manifold walks started at a point (black dot) inside a region converge to the associated solution (colored dot).

is a discrete and finite set⁵ of solutions connecting two given endpoints. Our approach to finding them is simple: whereas MNEE performs manifold walks using a fixed initialization, SMS randomly samples the initial guess from a probability distribution $p(\bar{x}_0)$. Newton’s method exhibits quadratic convergence when the starting point is sufficiently close to a root, hence all solutions will be found with a nonzero probability—however, the probability of successful convergence is unknown.

There is a great degree of latitude in the choice of an initial guess: we could uniformly generate positions on specular surfaces, or sample the BSDF of the preceding vertex x_1 and find starting points via ray tracing. Regardless of what approach is used, we assume that the implementation of this sampling strategy takes two uniformly distributed random numbers $\xi = (\xi_1, \xi_2) \in [0, 1]^2 =: \mathcal{U}$ as input and warps them to the desired distribution. Our objective now is to generate an initial sample ξ that is close enough to the solution, so that the Newton iteration (2) will take us there.

When inspecting the convergence behavior of these manifold walks on the *primary sample space* \mathcal{U} , we generally observe multiple *basins of convergence* $\mathcal{B}_k \subseteq \mathcal{U}$, each containing a point $\xi^{(k)}$ identified with a corresponding solution vertex $x_2^{(k)}$. Figure 4 illustrates the situation on a simple scene with a cardioid caustic. Newton’s method is known to produce convergence basins that potentially have an extremely complex geometric structure [Hubbard et al. 2001] and

⁵We note that cases with a continuous 1D subspace of solutions can be constructed, for instance when x_1 and x_3 lie at the center-line of a perfect cylindrical mirror. This is of no relevance for rendering natural scenes, since an arbitrarily small perturbation of the surface geometry would break the symmetries that are needed to create a 1D solution subspace. We ignore this corner case similarly to prior work [Walter et al. 2009].

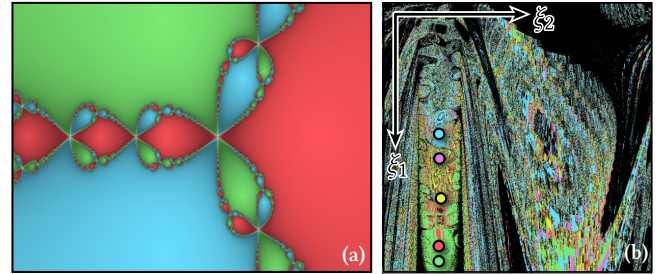


Fig. 5. (a): Newton fractal $z^3 - 1 = 0$. (b): Complex convergence basins with 5 unique solutions encountered in one of our scenes.

can even be fractal. For example, Fig. 5a shows convergence towards three different solutions of a simple polynomial equation on the set of complex numbers and Fig. 5b shows a particularly challenging convergence plot that we encountered after applying a normal map to the RING scene shown in Fig. 4. Recall that our goal is to use these solutions in a Monte Carlo estimator, where an algorithm that merely finds solutions is insufficient—we must also know the discrete probability p_k of finding a particular path vertex $x_2^{(k)}$. An unbiased estimator is then given by a standard MC ratio $f(\bar{x})/p(\bar{x})$, where $p(\bar{x})$ in the denominator contains p_k .

Since the samples ξ are uniformly distributed, this probability is simply the area of the associated convergence basin on \mathcal{U} :

$$p_k = \int_{\mathcal{U}} \mathbb{1}_{\mathcal{B}_k}(\xi) d\xi. \quad (4)$$

However, exact evaluation or precomputation of this integral is clearly infeasible: as discussed, \mathcal{B}_k can have an extremely complex shape which also depends on the position of the path endpoints. On the other hand, a simple unbiased estimator is given by

$$\langle p_k \rangle = \frac{1}{N} \sum_{i=1}^N \mathbb{1}_{\mathcal{B}_k}(\xi_i), \quad (5)$$

where $\xi_i \in \mathcal{U}$ is a sequence of i.i.d. uniform variates. Unfortunately, this approach is flawed: usage of p_k occurs in the *denominator* of the path throughput weight. Since $\mathbb{E}[1/X] \neq 1/\mathbb{E}[X]$, using this estimator could introduce significant bias: for example, $\langle p_k \rangle$ can equal zero if all N tries fail to converge to the basin \mathcal{B}_k , in which case the estimated path throughput weight would be infinite! Fortunately, an unbiased estimator for the inverse $\langle 1/p_k \rangle$ can be created using a simple iterative approach.

4.2 Unbiased SMS

The problem of computing an unbiased MC estimate of the reciprocal of an integral was studied by Booth [2007]. Recently, Qin et al. [2015] built on this idea to create an unbiased photon gathering strategy. The key idea underlying Booth’s approach is surprisingly simple: turning the inverse into a geometric series moves the problematic integral from the denominator to the numerator:

$$\frac{1}{p_k} = \frac{1}{\int_{\mathcal{U}} \mathbb{1}_{\mathcal{B}_k}(\xi) d\xi} = \frac{1}{1-a} = \sum_{i=0}^{\infty} a^i, \quad (6)$$

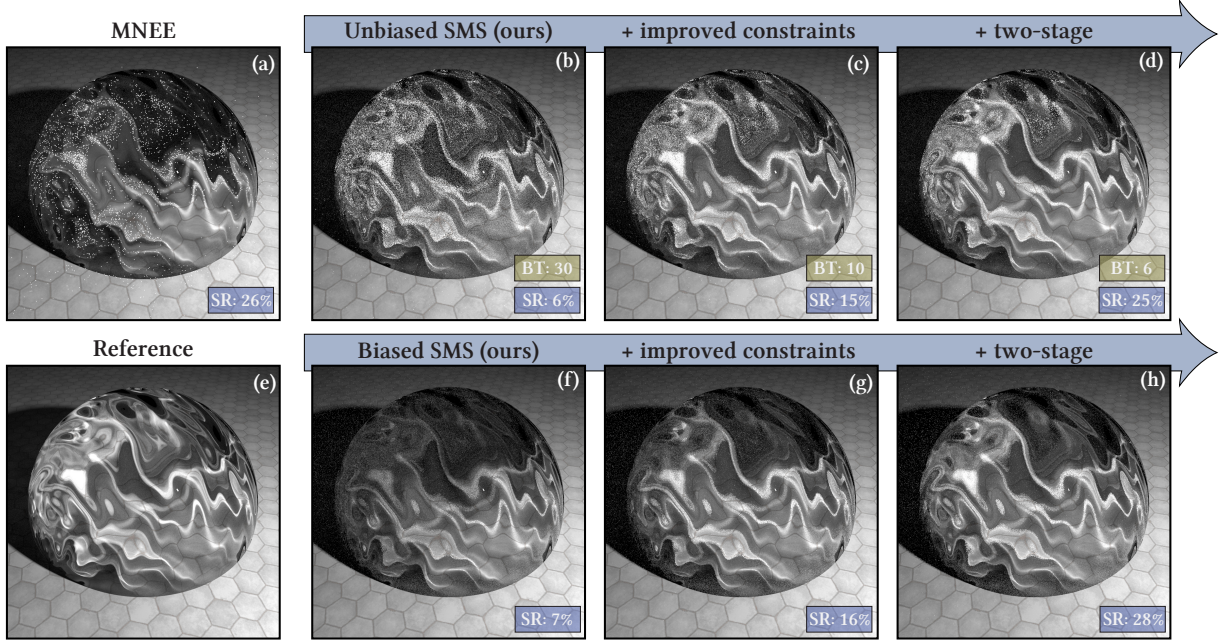


Fig. 6. Our two methods and their extensions illustrated on a normal-mapped dielectric sphere illuminated by a small area light; equal-time renderings (1 minute). Small insets summarize manifold walk success rate (SR) and average number of Bernoulli trials (BT), where applicable. (a): Previous work (MNEE) fails to capture the full complexity of the caustic as it only finds at most one refractive path per shading point. For the remaining energy it falls back to path tracing with high variance. (b): Our unbiased SMS method on its own. (c) - (d): Adding the constraint and two-stage manifold walk improvements which increase the success rate while reducing the iteration count. (f) - (h): Same sequence but using our biased SMS variant which suppresses the noise of the reciprocal probability estimation. As the success rate increases from left to right, bias goes down. The remaining bias mainly manifests itself in the regions where the unbiased counterpart remains noisy. The biased version uses a sample set size of $M = 16$. (e): The path-traced reference was rendered for 5 hours.

where $a = 1 - \int_{\mathcal{U}} \mathbf{1}_{\mathcal{B}_k}(\xi) d\xi$. This expansion is legal as long as $|a| < 1$, which in our case—integrating an indicator function over the unit square—is clearly satisfied. Unbiased estimation of the reciprocal then entails repeated manifold walks with i.i.d. initial points, denoted as $\langle a \rangle_j$ below:

$$\langle 1/p_k \rangle = 1 + \sum_{i=1}^{\infty} \prod_{j=1}^i \langle a \rangle_j. \quad (7)$$

Here, $\langle a \rangle_j = 0$ when manifold walk j has converged to root $\xi^{(k)}$ and $\langle a \rangle_j = 1$ if it has found another root or diverged. The above expression can thus be understood as a simple counting process: we run repeated manifold walks until $\xi^{(k)}$ is found, and the number of trials then provides an unbiased estimate of $1/p_k$. This result can also be understood in terms of the geometric distribution, which models the number of Bernoulli trials needed until a certain event with probability p_k takes place. Here again, the expected number of attempts is $1/p_k$. Simulating a geometric distribution therefore provides an unbiased estimator of the sought reciprocal and constitutes the base ingredient of our unbiased SMS scheme, which we lay out in Alg. 2.

Unbiased SMS is trivially added to any existing implementation of MNEE. Its runtime cost is directly linked to the “complexity” of specular paths in the scene: when the geometry is relatively smooth, \mathcal{U} contains a small number of solutions that are surrounded by large

ALGORITHM 2: Unbiased specular manifold sampling

```

Input: Shading point  $\mathbf{x}_1$  and emitter position  $\mathbf{x}_3$  with density  $p(\mathbf{x}_3)$ 
Output: Estimate of radiance traveling from  $\mathbf{x}_3$  to  $\mathbf{x}_1$ 
1  $\mathbf{x}_2 \leftarrow$  sample a specular vertex as initial position
2  $\mathbf{x}_2^* \leftarrow \text{manifold\_walk}(\mathbf{x}_1, \mathbf{x}_2, \mathbf{x}_3)$ 
3  $\langle 1/p_k \rangle \leftarrow 1$  ▷ Estimate inverse probability of sampling  $\mathbf{x}_2^*$ 
4 while true do
5    $\mathbf{x}_2 \leftarrow$  sample specular vertex as above
6    $\mathbf{x}'_2 \leftarrow \text{manifold\_walk}(\mathbf{x}_1, \mathbf{x}_2, \mathbf{x}_3)$ 
7   if  $\|\mathbf{x}'_2 - \mathbf{x}_2^*\| < \epsilon$  then
8     break
9    $\langle 1/p_k \rangle \leftarrow \langle 1/p_k \rangle + 1$ 
10 return  $f_s(\mathbf{x}_2^*) \cdot G(\mathbf{x}_1 \leftrightarrow \mathbf{x}_2 \leftrightarrow \mathbf{x}_3) \cdot \langle 1/p_k \rangle \cdot L_e(\mathbf{x}_3) / p(\mathbf{x}_3)$ 

```

convergence basins. Lines 1-2 then rapidly converge to a particular solution, and only a few iterations are required to find that same solution once more in lines 4-9. However, when the geometry is complex, many solutions may exist, and their convergence basins also occupy smaller area in primary sample space. The required number of trial iterations in lines 4-9 is a potential cause for concern in this case. Furthermore, the variance of such an estimator for a specific solution p_k based on a geometric distribution is equal to $(1 - p_k) / p_k^2$, which can become very large when $p_k \approx 0$.

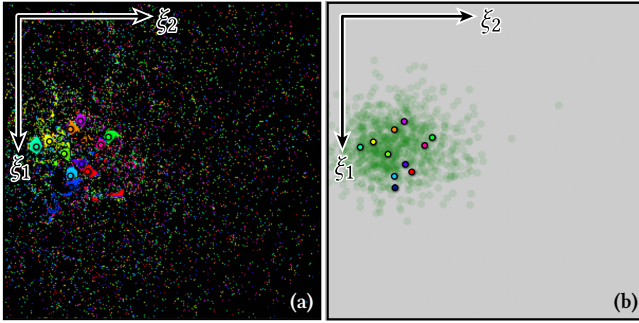


Fig. 10. (a): Convergence basins of the REFLECTIVE PLANE scene in Fig. 9a, for one shading point on the ground inside the caustic region. (b): Sampling density (green) of intermediate points after the first manifold walk in our two-pass approach, which focuses on the cluster of solutions.

paths on the original smooth surface. Such a smooth manifold walk will converge to a point that roughly lies at the center of the cluster of solutions in Fig. 10a. However, instead of an ordinary manifold walk, our first stage relies on an *offset manifold walk* [Jakob and Marschner 2012], whose manifold constraint tilts the normal of the underlying surface. The normal perturbation is randomly chosen from the distribution of normals that are present in the normal map. Cheaper approximations are also usable—we use a Gaussian approximation of the entire normal map obtained from the lowest MIP level of a LEAN map [Olano and Baker 2010]. Importantly, this offset normal is chosen before each manifold walk and does not change during the iteration which converges rapidly and with high probability (i.e. the convergence basin is large). This initial randomized manifold walk brings us into the proximity of the various solutions (green density in Fig. 10b); a second manifold walk, on the bumpy surface, started from there takes us all the way to a solution.

Estimation of the reciprocal probability of this adapted sampling strategy is surprisingly easy: the only requirement is that two-stage sampling is consistently used in both Lines 1-2 and Lines 4-9 of Alg. 2. It would generally appear that the two-stage sampling should be more costly, but in our experiments (e.g. Fig. 9) we observed roughly equal performance. The reason for this is that the reciprocal probability estimator requires fewer iterations to rediscover a solution. At the same time, variance is reduced noticeably.

4.6 Glints

Our method generalizes straightforwardly to the problem of rendering *glints*, which are minuscule subpixel reflections of a light source with narrow angular support (e.g. the sun) on high-frequency specular microgeometry. Rendering glints using standard Monte Carlo techniques tends to be prohibitively expensive, since millions of samples per pixel may be needed to obtain an acceptable result.

Interestingly, the problem of finding glints is almost identical to the caustic case, the main exception being that the search is now constrained to small surface regions observed by individual pixels and their reconstruction filters. Previous general glint rendering techniques [Yan et al. 2014, 2016] evaluate an effective integrated BRDF over the entire pixel footprint and produce very high quality

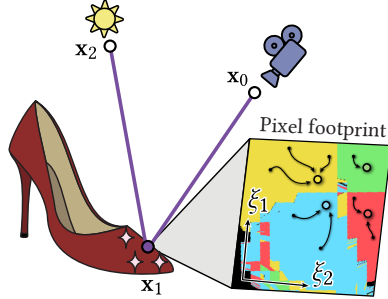


Fig. 11. Specular manifold sampling can also find connections within a pixel footprint to render glints that arise due to specular microstructure.

estimates at the cost of burdensome 4D spatio-directional hierarchies that are necessary to organize and query the distribution of normals. Our goal is to implement an unbiased estimate of such a query using manifold walks.

Our method generates random starting points within the pixel and then runs unbiased or biased SMS to find solutions (Fig. 11). In contrast to prior work, which introduced a small amount of *intrinsic roughness* to relax the problem, we solve the unmodified problem with a discrete set of solutions to find a path $\bar{x} = x_0, x_1, x_2$ connecting the camera to a sampled emitter position via a single⁷ specular reflection. After tracing the initial camera ray, we approximate the projected pixel footprint with a small parallelogram based on ray differentials [Igehy 1999]. We perform local manifold walks in UV space to refine the initial guess. This leads to much higher performance compared to the caustic case as no costly ray tracing operation is needed to re-project onto the surface. We terminate paths that step outside the parallelogram since they are unlikely to find usable solutions. Like prior work, we assume that the endpoints x_0 and x_2 are distant, in which case changes in the half-vector across the parallelogram are minimal. It can thus be approximated by a constant, which simplifies the search for solutions: in particular, the specular manifold constraint can be simplified to a function that attempts to equate this fixed half-vector and the local shading normal, both expressed in 2D slope space. Like previous work, we use high-resolution normal maps to encode the subpixel surface details in our scenes. In principle, the method could be extended to other types of normal variation or actual geometric displacement.

To robustly apply our glint rendering technique in scenes with complex lighting (e.g. high-frequency environment maps), we further combine our SMS strategy with standard BSDF sampling in a multiple importance sampling (MIS) framework. We found it very effective to use approximate MIS weights based on the directional distributions from the light source and the effective BSDF of the pixel footprint provided by a LEAN map. As shown in Fig. 12 this approach successfully separates the regions of the integrands where one sampling strategy is preferable over the other. While precomputing a LEAN map adds some storage overhead, it is orders of magnitude lower than Yan et al.’s spatio-directional trees. We also note that our method always renders the non-smoothed input normal map without geometric approximations—the LEAN map is only

⁷Glints involving multiple specular reflections on displaced geometry can in principle be found using our method and could be an interesting topic for future work.

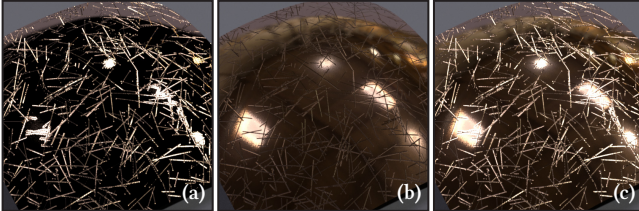


Fig. 12. Curved metal surface with small scratches lit by a high-frequency environment map containing multiple light sources. Weighting using multiple importance sampling (MIS) effectively uses each technique where it performs best: (a): Our method (unbiased SMS) captures the direct illumination from the bright light sources inside the scratches. (b): Standard BSDF sampling focuses on reflections from flat regions. (c): Combined result.

used as a proxy to compute an effective BSDF sampling density over a pixel footprint, enabling unbiased combination of our sampling strategy with other standard techniques via MIS.

4.7 Integration into rendering algorithms

Specular manifold sampling is a general building block in the design of rendering algorithms, and there is considerable flexibility in its usage. We experimented with different ways of incorporating it into a unidirectional path tracer and ultimately opted for uniform seed-point generation on specially marked “caustic caster” shapes. For two-bounce caustics, shown in Section 5, the seed point on the second interface is found by tracing a ray through the first vertex and performing either reflection or refraction depending on the type of surface. SMS is very effective for sampling high-frequency caustic paths from (near) specular surfaces and often greatly outperforms standard emitter or BSDF sampling strategies. However, in the case of significant surface roughness or smooth illumination, standard strategies remain superior. Ideally, all of these strategies would be combined via MIS to improve their robustness, as we do in Section 4.6 for the special case of glints. However, determination of suitable probabilities in the more general caustic setting remains an open problem. SMS iterations are also relatively expensive, and we use them even at shading points where no possible connections exist. Conservative criteria that specify when SMS should be used are another interesting avenue for future work.

5 RESULTS

We now present several results rendered with our method as well as comparisons to relevant prior work. We based our implementation on the Mitsuba 2 renderer [Nimier-David et al. 2019]. All time measurements in this article were recorded on a compute node with 2 Xeon 6132 processors, each with 14 2.6 GHz cores. Many of the rendered results contain small insets with the manifold walk success rate (SR) for the corresponding image. These numbers may seem low at first, but are averaged over the full image—including pixels that do not contain any caustics for SMS to find.

Many of the results below are additionally shown in animated form as part of the supplemental video:

- Comparison of SMS against prior work on three scenes (Fig. 14): SWIMMING POOL, REFLECTIVE PLANE, and REFRACTIVE SPHERE.

- Temporal coherency and the effect of the trial set size M in biased SMS (Fig. 15).
- Two-bounce refractive caustics in the DOUBLE-REFRACTIVE SLAB scene (Fig. 18).
- Temporal coherency of SMS on glints in the SHOES and KETTLE scenes (Fig. 19).

5.1 Shop window scene

Figure 1 showcases our method in an example involving glints and caustics on complex geometry. It features several different caustics rendered using unbiased SMS: reflective caustics caused by a spotlight shining on the gold pedestals, and a two-bounce refractive caustic from a point light hidden inside the middle pedestal. The shoes have a glittery appearance that is rendered using biased SMS for glints. We disable caustics from higher order scattering (e.g. two or more bounces between the pedestals). Many of the caustics in this scene are SDS paths that a regular path tracer cannot find. We can still compare to a path tracer by adding some surface roughness (Beckmann NDF with $\alpha = 0.005$) to all specular shapes. Figure 13 shows such a comparison, where we only visualize the contributions sampled by SMS. Given equal render time, our method outperforms regular path tracing by a significant margin.

The scene also illustrates a current limitation of our method: even though SMS can effectively sample light connections through specular interfaces, there is still significant variance in the scene coming from other challenging paths, mainly the indirect lighting caused by the caustics; see Fig. 13b and the remaining noise in Fig. 1. Our method cannot sample these paths explicitly; the issue could be addressed by path guiding methods.



Fig. 13. Modified version of the SHOP WINDOW scene from Fig. 1 where a small amount of surface roughness is added to the previously purely specular surfaces, enabling a standard path tracer (a) to find the same light transport paths as our proposed method (b). Both renderings are computed in equal time (20 minutes), showing only contributions due to caustics.

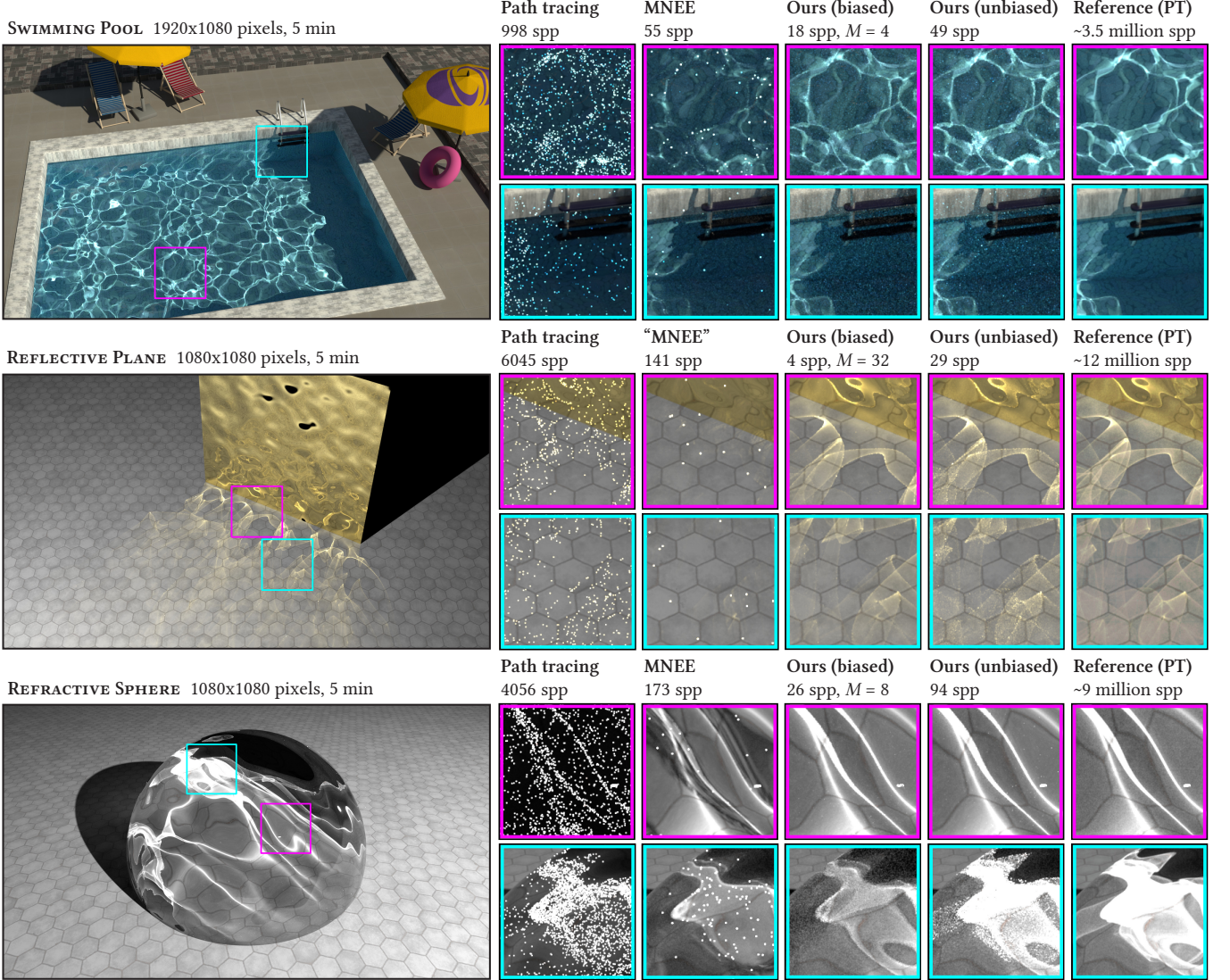


Fig. 14. Equal-time comparison (5 minutes) between path tracing, prior-work MNEE [Hanika et al. 2015a], and both unbiased and biased versions of our proposed SMS method. Previous work can only produce (at most) one connection to the light source via the specular interface, whereas our techniques can sample the full range of light paths either in an unbiased or biased way. The latter removes some of the high-frequency noise introduced by unbiased probability estimation and trades it for energy loss with the trial-set size parameter M . We report samples per pixel (spp) computed by each method, as well as the chosen M in the biased case.

5.2 Specular manifold sampling

In Fig. 14 we compare the effectiveness of SMS to brute-force path tracing and the previous state-of-the-art method MNEE of Hanika et al. [2015a]. We examine three scenes with challenging caustics due to normal-mapped surfaces. The SWIMMING POOL and REFRACTIVE CAUSTIC scenes are a famous examples where both uni- and bidirectional path tracing techniques fail to discover the prominent SDS paths that generate intricate patterns on the ground plane. MNEE improves on this but misses all but one light connection. For the remaining paths it has to either fall back to the brute-force strategy that has significant variance still or suffers from severe

energy loss if those light connections are omitted. Our method finds all paths and significantly outperforms the others in equal time.

The REFLECTIVE PLANE scene is an example where MNEE was previously not applicable. For a clearer comparison, we added a variation (called “MNEE” in quotes) that constructs a deterministic seed path by tracing a ray from the shading point towards the center of the object’s bounding box. Since the caustic is the superposition of many individual solutions, this is clearly not sufficient and “MNEE” ends up finding only a very small part of the caustic. Biased versions of SMS can optionally be applied and reduce high-frequency noise caused by the unbiased probability estimate. This comes at a higher

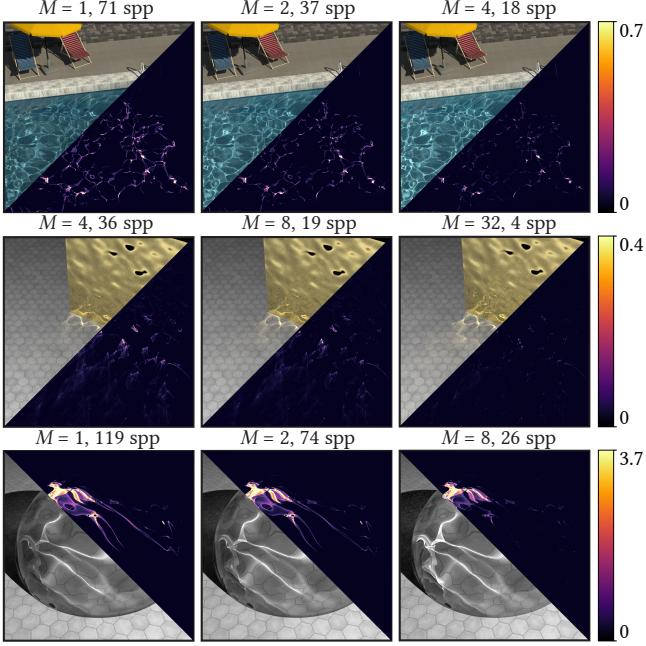


Fig. 15. Comparing our biased method with varying trial set sizes M , at equal render time of 5 minutes. As M increases, each individual radiance estimate becomes more expensive but less energy of the caustics is lost. Overlays show pixel-wise squared error compared to unbiased SMS.

cost per individual sample and some energy loss, the extent of which can be controlled by the trial set size M . We want to highlight that the biased method is free of artifacts and generates temporally coherent results despite its limited exploration of a random subset of the path space. Animated results of this comparison for different values of M are shown in the supplemental video.

5.3 Biased SMS

Our biased SMS approach involves an interesting tradeoff between sample variance and energy loss. The trial set size parameter M plays an important role here: it directly relates to how much effort the sampler spends per radiance estimate from caustics, and indirectly controls how much of the caustic is found. We explore this effect in Fig. 15 on the same scenes as used above. Choosing the optimal M is currently a user choice and could be investigated more in the future.

5.4 Geometric displacement

Although many of the shown results involve caustics from specular surfaces with normal maps, our method is more general, and we also found it to be effective on surfaces with true geometric detail (e.g. from a displacement map), which we illustrate in Fig. 16. When not using our two-stage sampling method, which is currently limited to normal maps, manifold sampling performs equally well on both types of surfaces as confirmed by the similar success rates. This seems counter-intuitive at first, since smoother geometry should also result in a specular manifold that is easier to navigate. However,

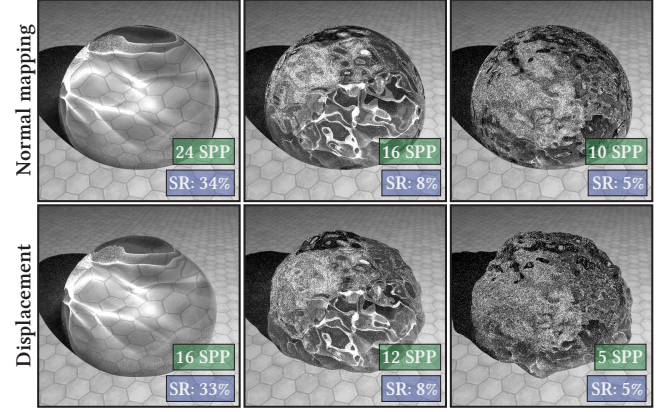


Fig. 16. **Top:** Sequence of refractive spheres with increasingly complex normal maps. **Bottom:** The same setup, but this time with actual displaced geometry. Insets show computed number of samples per pixel (SPP) and the manifold walk success rate (SR) measured over all pixels in the image. The manifold walks perform about equally on both geometry types.

the disagreement between actual geometry and the “fake” surface variation from normal maps can also limit the Newton solver’s efficiency. The ray-tracing-heavy nature of the manifold walks and the underlying re-projection steps lead to slightly reduced performance in scenes with dense geometric tessellation.

5.5 Surface roughness

Like prior work on specular manifolds, our method generalizes to near-specular or rough surfaces by performing offset manifold walks previously described in Section 4.5. Here, we sample an *offset normal* from the material’s microfacet distribution before the SMS step. The manifold walk then searches for specular connections involving that offset normal instead of the true shading normal. Only a finite number of solutions exists for this specific offset normal, and the probability estimate of therefore remains unchanged. Averaging over paths sampled in this manner converges to the correct solution [Hanika et al. 2015a].

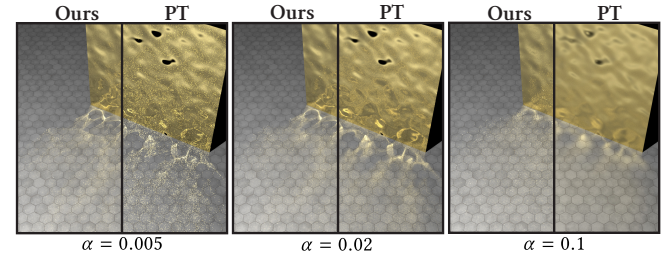


Fig. 17. Rough reflective plane with a rough metallic surface with Beckmann normal distribution. As the roughness increases from left to right, the path tracer (PT) becomes more capable of performing the connection to the light source on specular plane directly, whereas our proposed sampling strategy loses its efficiency. Both methods use equal render time of 5 minutes.

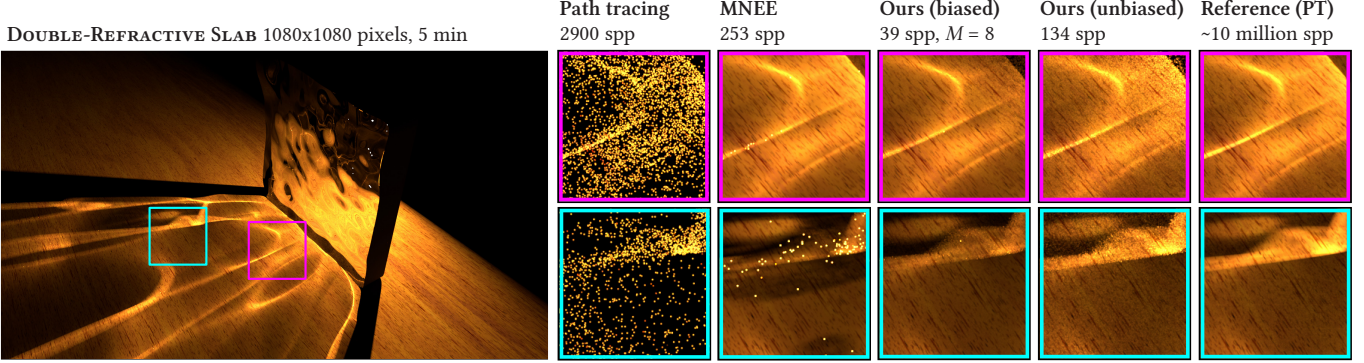


Fig. 18. Equal-time comparison (5 minutes) of our method on a challenging scene where SMS samples a light connection involving two consecutive specular refractions. The two-sided solid piece of glass is modeled with geometric displacement.

Figure 17 shows a sequence of increasingly rough reflective surfaces. Note how the caustic is at first sharp and full of high-frequency details, and becomes progressively blurry from left to right. This blur also enables a unidirectional path tracer to find valid light connections more often: in the limit case, every point on the surface is contributing to the shading point. As our method handles roughness by integrating over many perfectly specular light paths with randomized offset normals, the opposite is true for our method and its variance increases. We only recommend using our technique for specular or near-specular surfaces and switching over to conventional path sampling techniques in other cases. In the future, it would be interesting to incorporate a form of multiple importance sampling to robustly handle both extremes in addition to intermediate cases. Note that the same argument applies also to scenes with low-frequency lighting, e.g. largely constant environment maps.

5.6 Multiple specular interactions

Like MNEE, the principle behind our method generalizes to longer chains with multiple specular interactions. In Fig. 18, we show an intricate caustic pattern caused by double refraction through a solid displaced piece of glass. We again compare our unbiased and biased SMS variants to a standard path tracer and MNEE. Multiple interactions increase the dimension of the space of initial configurations that SMS must generate: we could generate initial rays to start the manifold walks in the same way as before, but at each interaction we additionally decide between reflection or refraction (if applicable), and whether or not to terminate the chain and attempt to connect to a light position. To keep variance manageable we found it best to limit SMS to a single family of light paths in this setting (e.g. paths of fixed length with only refractive events). In cases where this increased variance is not acceptable, the biased technique can still be applied—but for the same reasons there will be a potentially significant energy loss. As shown in the DOUBLE-REFRACTIVE SLAB scene, SMS can still produce good results, but better strategies for sampling initial configurations will be required to turn SMS into a fully general sampling strategy that can efficiently find *all possible* chains of specular interactions.

5.7 Glints

Figure 19 examines the performance of our glint rendering technique on two scenes with complex microstructure specified using normal maps. We compare our SMS to the state-of-the-art method of Yan et al. [2016]. Both methods make use of MIS in this comparison. The SHOES scene features a glittery pair of shoes with procedural normal displacement by a Gaussian height field and is lit by a sky with an almost purely directional sun. The KETTLE scene involves brushed metal with very strong anisotropy. It is illuminated by the Grace Cathedral environment map, which includes several bright and narrow light sources. Stochastic sampling of glint solutions is beneficial in these cases, since several complementary sources of variance can be reduced at the same time.

We found the biased SMS variant to generally be more practical for glint rendering compared to its unbiased counterpart.⁸ The potentially unbounded number of iterations in the recursive unbiased probability estimator, combined with extremely high-frequency normal map detail, occasionally produces acute outliers in the pixel estimate that lead to poor convergence, as seen in the plots.

Note that all methods in Fig. 19 converge to slightly different results, but they all find the same individual glints and have very similar appearance overall. Our method uses 100–300× less memory compared to previous work (e.g. 110 MiB vs. 11 GiB). At the same time, it converges in an equal or shorter amount of time and still generates temporally coherent animations. Please see the supplemental video for an animated demonstration.

6 CONCLUSION

We introduced a simple and powerful specular path sampling technique that combines deterministic root finding with stochastic sampling in a pure Monte Carlo setting. The basic method can be used in a variety of different ways, and we demonstrated example applications in the context of efficient path tracing of glints and caustics. Our approach is not restricted to unidirectional path tracing, and we contemplate its utility in bidirectional and even MCMC methods, where manifold walks were originally proposed.

⁸The bias here only involves the probability estimate. In practice, even the “unbiased” version will not match a brute-force result perfectly due to the far-field approximation.

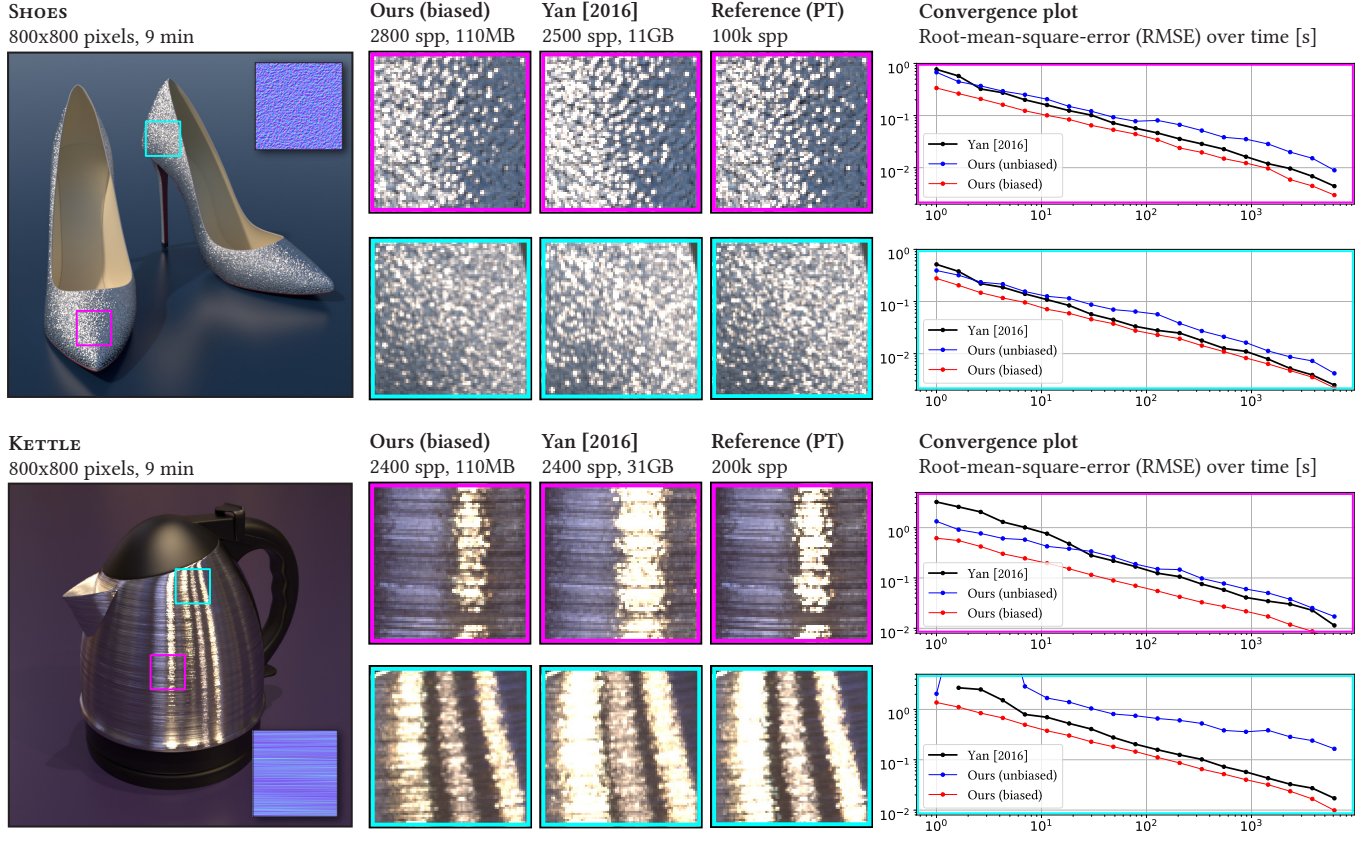


Fig. 19. Equal-time comparison (9 minutes) of our glint rendering method to prior work specific to this problem [Yan et al. 2016]. SHOES scene: highly directional illumination from the sun, KETTLE scene: grace cathedral environment map where integration over multiple sources of variance (i.e. all the lights) is critical. Our method yields comparable results in the first scenario and is superior in the second. At the same time, our method requires 100–300× less memory. The insets and corresponding convergence plots focus on different parts of the glinty appearance.

Building on a simple unbiased algorithm, we presented several complementary extensions and improvements. For example, better strategies for sampling seeds paths can further improve convergence, and such heuristics are easy to integrate into our method without introducing bias. Improved manifold constraints expand the size of the convergence basins in primary sample space. A further change yields an intentionally biased estimator with desirable properties for production usage. Far-field approximations in the context of specular glints lead to a particularly simple iterative algorithm, whose steps no longer require the use of ray tracing operations. In the future, we would like to explore further acceleration of this variant leveraging vectorized execution.

Determining *when* to use our method is another important aspect for future investigation. Attempting many connections that are ultimately unsuccessful can consume a large amount of computation. While glints would benefit from simple culling heuristics, e.g. based on cones bounding the normal variation inside the pixel, the general case of caustics from arbitrary specular geometry is significantly more challenging. Combining our techniques with others via multiple importance sampling in this general setting is another pertinent problem.

Our article focuses mainly on the generation of subpaths with a single specular vertex. While our method in principle also generalizes to more complex path classes with multiple specular reflection, performance using our current strategy for choosing starting points remains suboptimal and could be an interesting topic for future work. We wish to pursue these and related improvements, and envision a unified path sampling strategy that elevates stochastic manifold walks to a standard building block in the design of Monte Carlo rendering methods.

ACKNOWLEDGMENTS

We thank Guillaume Loubet for many insightful discussions about glints and caustics, Olesya Jakob for designing the shop window scene in Fig. 1, and Ling-Qi Yan and Miloš Hašan for sharing their implementation of prior work [Yan et al. 2016].

Our test scenes use textures from CC0 Textures and cgbook-case, and are lit by environment maps courtesy of HDRI Haven and Paul Debevec. The kettle model in Fig. 19 has been created by Blend Swap user *PrinterKiller*.

This work was funded by a grant from Autodesk.

